HIF-1α and HIF-2α transcription factors differentially regulate lung alveolar macrophage function

Authors: Elena Priego[1,2]*, Irene Adán-Barrientos[1,2,3]*, Ruth Conde-Garrosa[1], Sarai Martínez-Cano[1,4], Iria Sánchez[1], Diego Mañanes[1,2], Annalaura Mastrangelo[1], Joaquín Amores[1], Helena M. Izquierdo[4#] and David Sancho[1#].

[1]Centro Nacional de Investigaciones Cardiovasculares Carlos III

[2]Escuela de Doctorado, Universidad Autónoma de Madrid.

[3]Departamento de Inmunología, Oftalmología y ORL, Facultad de Medicina, Universidad Complutense de Madrid

[4]Inmunotek S.L. Alcalá de Henares, Madrid

[5]Institut Curie, PSL University, INSERM U932, Immunity and Cancer, Paris, France.

*Co-first authors.

[#]Senior and corresponding authors: helena.izquierdo-fernandez@curie.fr; dsancho@cnic.es;

ABSTRACT

Alveolar Macrophages (AMs) reside in the alveoli, where oxygen pressure is high, therefore maintaining an active degradation of hypoxia-inducible transcription factors (HIF) mediated by the Von Hippel-Lindau protein (pVHL) ubiquitin ligase complex. We previously found that *Vhl*-deficient AMs not sensing high oxygen pressure are immature and functionally impaired. Here we investigated the specific roles of HIF-1α and HIF-2α isoforms in the regulation of AM functions. With this aim, we combined deletion of *Vhl* with single or double deletion of *Hif1a* and/or *Hif2a* in AMs under the control of the CD11c promoter using a Cre-Lox system. Our work demonstrates that in *Vhl*-deficient macrophages, both HIF-1α and HIF-2α contribute to AM defective self-renewal, while HIF-2α plays a central role in regulating the impaired AM maturation associated with pVHL loss. HIF-1α promotes a glycolytic shift in alveolar macrophages, while HIF-2α hinders lipid oxidation and surfactant clearance. Thus, HIF-2α raises as a selective critical factor restraining the therapeutic potential of AMs to degrade surfactant excess in mice that have

developed pulmonary alveolar proteinosis (PAP). Overall, regulation of both HIF-1α and HIF-2α isoforms is required for an optimal AM function, highlighting HIF-2α as a potential pharmacological target for secondary PAP.

INTRODUCTION

Alveolar macrophages (AMs) are lung-resident cells maintained by self-renewal during homeostasis.[1] Through the sensing of granulocyte-macrophage colony-stimulating factor (GM-CSF) [2,3] and transforming growth factor β (TGF-β),[4] fetal liver monocytes differentiate into mature AMs in the lung alveoli during the first week of life**.** Mature AMs are essential for the regulation of surfactant in the lung, which is comprised of 90% lipids and is required to decrease surface tension. AMs have a remarkable ability for lipid catabolism and cholesterol handling,[5] and these functions are sustained by enzymes and receptors whose expression is regulated by Liver-X family of receptors (LXRs), Peroxisome proliferator-activated family of receptors (PPARs), CCAAT enhancer-binding proteins (C/ EBPs), and sterol regulatory element-binding proteins (SREBPs) transcription factors.[6] Changes in AM lipid metabolism are found in human respiratory diseases such as chronic obstructive pulmonary disease (COPD) [6] and pulmonary alveolar proteinosis (PAP).[7,8] Mechanistically in mice, deletion of *Pparg*, a master regulator of lipid metabolism induced by GM-CSF, selectively impairs the differentiation of Ams.[3] Depletion of the transcription factor TFAM, involved in mitochondrial biogenesis, leads to a reduction in AM numbers and impairs their maturation *in vivo.* [5,9] Overall, these studies have identified essential factors required for AM maturation and function and demonstrate that alterations of AM metabolism are associated to AM dysfunction. We have previously shown that pVHL is necessary for the adaptation of AMs to high oxygen levels upon birth, and that *Vhl* deletion renders immature and functionally impaired AMs, which also present an altered metabolic profile, including enhanced glycolysis and decreased lipid oxidation capacity.[10] However, the role of each HIFα isoform in regulating the functional maturation of AMs has not been investigated.

pVHL is the substrate recognition unit of an E3 ubiquitin ligase complex involved in the ubiquitination and degradation of the alpha isoforms of hypoxia inducible factors (HIFs) in an oxygen dependent manner.[11–13] HIFs are heterodimeric transcription factors that induce the expression of a set of genes functionally involved in the cellular adaptation to low oxygen tension or hypoxia, including the metabolic switch to glycolysis.[14,15] HIFs are composed of an oxygen sensitive α subunit and a constitutive β subunit. Three α subunits have been described (HIF-1α, HIF-2α, and HIF-3α), which heterodimerize with HIF-1β subunit (also named Aryl Hydrocarbon Receptor Nuclear Translocator 1; ARNT1), forming HIF-1, HIF-2 and HIF-3 transcription factors,

respectively.[16] When dimerized with the HIF-1β subunit, HIF-1α and HIF-2α regulate the transcription of both shared and distinct target genes. HIF-3α acts as a negative regulator of HIF-1α and HIF-2α by competing for HIF-1β protein available for dimerization, although the HIF-3 dimer also induces the expression of specific target genes.[17] Beyond HIFα regulation, pVHL plays a role in other cellular processes including cytokine signaling, regulation of senescence, formation of extracellular matrix and mitochondrial function.[18–25] Notably, in our previous work, we found that genes related to the adaptation to hypoxia, including many targets of HIF-1α and HIF-2α, were downregulated within AM maturation after birth.[10] Therefore, we hypothesize that HIF-1α and HIF-2α must be degraded to ensure the correct functional maturation of AMs in steady-state.

Here, we investigated the specific function of HIF-1α and HIF-2α in AM phenotypic maturation, self-renewal and surfactant clearance in the lung. To assess this, we generated four different strains of mice: CD11c-Cre *Vhl*$^{fl/fl}$ (CD11c∆*Vhl*), CD11c-Cre *Vhl*$^{fl/fl}$*Hif1a*$^{fl/fl}$ (CD11c∆*Vhl*∆*Hif1a*), CD11c-Cre *Vhl*$^{fl/fl}$*Hif2a*$^{fl/fl}$ (CD11c∆*Vhl*∆*Hif2a*) and CD11c-Cre *Vhl*$^{fl/fl}$*Hif1a*$^{fl/fl}$*Hif2a*$^{fl/fl}$ (CD11c∆*Vhl*∆*Hif1a*∆*Hif2a)*. We demonstrate that expression of either HIF-1α and HIF-2α alone is sufficient to intrinsically and differentially impair AM terminal maturation and self-renewal, with full rescue observed only in CD11c∆*Vhl*∆*Hif1a*∆*Hif2a* mice. Whereas HIF-1α drives AM metabolic shift towards glycolysis, HIF-2α disrupts lipid oxidation and surfactant clearance, and is the main isoform responsible for impaired AM maturation. Altogether, this study shows that HIF inactivation ensures the optimal maturation of AMs in the lung, regulating the metabolic adaptation to high oxygen concentration and highlights different functional specificities of each HIFα isoform.

RESULTS

HIF-1α is the driver of the metabolic switch to glycolysis in pVHL-deficient alveolar macrophages

Our previous work established that pVHL is required for AM phenotypic and functional maturation,[10] but did not address the specific contribution of HIF-1α and HIF-2α or additional effects of pVHL. To analyze the specific function of HIF-1α and HIF-2α in AMs, we generated four different mouse strains: CD11c-Cre *Vhl*$^{fl/fl}$ (CD11c∆*Vhl*), CD11c-Cre *Vhl*$^{fl/fl}$*Hif1a*$^{fl/fl}$ (CD11c∆*Vhl*∆*Hif1a*), CD11c-Cre *Vhl*$^{fl/fl}$*Hif2a*$^{fl/fl}$ (CD11c∆*Vhl*∆*Hif2a*) and CD11c-Cre *Vhl*$^{fl/fl}$ *Hif1a*$^{fl/fl}$*Hif2a*$^{fl/fl}$ (CD11c∆*Vhl*∆*Hif1a*∆*Hif2a)*. Analysis of AMs from these mice revealed the expected genotype deficiencies in *Vhl*, *Hif1a*, and *Hif2a* expression (**Error! Reference source not**

93 **found.**A-C), with additional half reduction in *Hif1a* expression levels in CD11c∆*Vhl*∆*Hif2a* mice
94 (**Error! Reference source not found.**B).

95 To investigate the contribution of HIF-1α and HIF-2α to the immature-like phenotype found in *Vhl*-
96 deficient Ams,[10,26] we performed an RNA-seq of AMs isolated from all the mice strains compared
97 with their respective Cre negative littermate control mice. Analysis of differentially expressed
98 genes (DEG) showed 1246 genes expressed with at least a 2-fold difference (Adj. $p < 0.01$)
99 between each conditional KO and its control, except for CD11c∆*Vhl*∆*Hif1a*∆*Hif2a* AMs, in which
100 only *Vhl* and *Plcb4* were differentially expressed (Figure 1A-D), showing that the transcriptional
101 changes seen in *Vhl*-deficient AM relies exclusively on downstream transcription factors HIF-1α
102 and HIF-2α rather than on HIF-independent pVHL functions. Principal Component Analysis (PCA)
103 showed that samples from CD11c∆*Vhl*∆*Hif1a*∆*Hif2a* scored close to controls and distant from
104 CD11c∆*Vhl*, CD11c∆*Vhl*∆*Hif1a*, and CD11c∆*Vhl*∆*Hif2a* in principal component 1 (PC1) (Figure
105 1E).

106 Different genes were deregulated in AMs depending on the genotype (**Error! Reference source**
107 **not found.**A-C). Pre-ranked enrichment analysis of the genes with the greatest contribution to
108 PC1 unveiled pathways related with cell division and metabolism, especially glucose related
109 pathways, suggesting that both HIF-1α and HIF-2α are involved in their regulation (Figure 1F). To
110 further interrogate the specific contribution of each HIF isoform, we performed an
111 overrepresentation analysis, using the Gene Ontology (GO) database, of DEG from each
112 genotype. Most of the downregulated pathways in *Vhl*-deficient AMs were restored upon further
113 deletion of *Hif1a* and not *Hif2a*, such as cell cycle, DNA replication, p53 signaling pathway or fatty
114 acid (FA) metabolism (**Error! Reference source not found.**D). We also found pathways similarly
115 controlled by HIF-1α and HIF-2α such as *AMPK signaling pathway* or *PI3K-Akt signaling pathway*
116 (**Error! Reference source not found.**D), suggesting that binding of either HIF isoform to the
117 same gene promoters is sufficient to activate these pathways. In contrast, *PPAR signaling*
118 *pathway*, *HIF1A signaling pathway* or *Glycolysis/Gluconeogenesis* pathways were only partially
119 restored by HIF-1α or HIF-2α deficiency, indicating their differential regulation by both
120 transcription factors (**Error! Reference source not found.**D).

121 HIF-1α and HIF-2α induce the transcription of common target genes involved in the response to
122 hypoxia. However, stable activation of HIF isoforms with prolonged hypoxia can result in the
123 predominance of HIF-2α activity rather than HIF-1α.[27] To characterize the contribution of each
124 HIF isoform to these specific pathways in *Vhl*-deficient AMs, we compared the core gene
125 expression signature associated with the response to hypoxia KEGG pathway. The upregulated

genes found in *Vhl*-deficient AMs were restored by further deletion of *Hif1a* but not *Hif2a* (**Error! Reference source not found.**E). The same was true for DEGs associated to oxidative phosphorylation (OxPhos) and Glycolysis pathways (**Error! Reference source not found.**F-G), suggesting that HIF-1α is the main regulator of these genesets over HIF-2α in AMs. We also found that deleting *Hif2a* in *Vhl*-deficient AMs further amplified the transcriptional changes associated to the response to hypoxia, observed in *Vhl* deletion alone (**Error! Reference source not found.**F-G). This suggests a negative role of *Hif2a* in the regulation of these pathways. Real-time metabolic profile of AMs in the presence of glucose, pyruvate, and glutamine by Seahorse showed that CD11c∆*Vhl* and CD11c∆*Vhl*∆*Hif2a* AM significantly decreased the basal respiratory rate (BRR) while maintaining extracellular acidification rate (ECAR) compared to controls, reflecting a decreased use of glucose for TCA and mitochondrial oxidative phosphorylation (OxPhos) towards an enhanced aerobic glycolysis and lactate production. In contrast, CD11c∆*Vhl*∆*Hif1a* and CD11c∆*Vhl*∆*Hif1a*∆*Hif2a* AM showed levels of BRR and ECAR similar to WT (Figure 1G-H). Overall, our results suggest that the transcriptional program governing AM response to hypoxia, including genes related to OxPhos and glycolysis, is regulated by HIF-1α. Consistent with this, HIF-1α emerges as the key driver of the metabolic switch towards glycolysis in *Vhl*-deficient AMs.

HIF-1α and HIF-2α differentially regulate AM identity genes in pVHL-deficient mice

We have previously shown that Vhl-deficient AM showed an altered expression of surface markers,[10] akin to immature cells.[2] We then asked which HIF isoform dampens mature AM identity in the absence of pVHL. We compared the expression level of classical surface markers that are associated with AM maturation status. While the expression pattern of maturation markers such as CD11c, SiglecF, CD11b or MHC class II (I-A/I-E) was restored to control WT levels in CD11c∆Vhl∆Hif1a∆Hif2a, most of the changes in marker expression found in CD11c∆*Vhl* mice remained unchanged upon further depletion of HIF-1α. In contrast, these changes were largely reversed upon HIF-2α depletion (Figure 2A-E), suggesting that HIF-2α plays a central role in regulating the impaired AM maturation associated with pVHL loss. We then compared the unique AM gene expression signature that was identified by the Immgen consortium. [28] Notably, we found three distinct sets of genes: (i) genes regulated by HIF-2α, with functions in lipid metabolism (Lsr, Vstm2a, Cidec), (ii) genes regulated by HIF-1α, involved in a plethora of functions including regulation of cytoskeleton (Clmn, Sema3e, Krt19, Matn2, Itgax), circadian clock genes (Ear1, Rara) and cell metabolism (Lepr, Naaa, Acaa1b, Aldoc, Fabp1); and (iii) a third set of genes regulated by both HIF-1α and HIF-2α (Figure 2F). Overall, our data indicate that while deleting HIF-2α in Vhl-deficient AMs fully restores the control WT surface marker expression, both HIF

159 isoforms contribute either individually or together shape the subjacent transcriptional identity of
160 mature AMs (Figure 2F).

161 **AM self-renewal capacity is impaired by both HIF-1α and HIF-2α in pVHL-deficient mice**

162 AMs are lung resident cells maintained locally by self-renewal in steady-state.[29] Enhanced
163 glycolysis has been correlated with reduced AM self-renewal capacity,[5,10,26] but its association
164 with specific HIF-1 isoforms remains unclear. Thus, we next investigated which HIF isoform was
165 regulating AM proliferation in *Vhl*-deficient AMs. The frequency of Ki67$^+$ AMs was significantly and
166 similarly reduced in CD11c∆*Vhl*∆*Hif1a* and CD11c∆*Vhl*∆*Hif2a* AMs, indicating that both isoforms
167 contribute to the defective proliferation in the absence of pVHL (Figure 3A). In contrast, it was
168 completely restored to control WT in CD11c∆*Vhl*∆*Hif1a*∆*Hif2a* AMs (Figure 3A). In agreement,
169 the differential expression of genes associated to cell cycle in CD11c∆*Vhl* AM was not restored
170 by the additional single deletion of *Hif1a* or *Hif2a*, being reverted only in CD11c∆*Vhl*∆*Hif1a*∆*Hif2a*
171 AMs (**Error! Reference source not found.**A). Furthermore, BrdU uptake in *ex vivo* AM cultures
172 with GM-CSF show a recovery of their full proliferative capacity only in the *Vhl/Hif1a/Hif2a* triple
173 knockout (Figure 3B). Overall, these results demonstrate that HIF-1α and HIF-2α impair AM
174 stemness independently of glycolysis and of environmental extrinsic factors.

175 AMs can differentiate from circulating monocytes coming from bone marrow precursors.[29] We
176 then asked whether the previously observed compromised AM proliferative capacity constitutes
177 a selective disadvantage at reconstituting an empty niche in a context of competence with WT
178 AM. To address this, we generated bone marrow mixed chimeras: lethally irradiated CD45.1$^+$
179 recipients were transferred intravenously with bone marrow cells from CD45.1$^+$CD45.2$^+$ WT
180 control and CD45.2$^+$ CD11c∆*Vhl*, CD11c∆*Vhl*∆*Hif1a*, CD11c∆*Vhl*∆*Hif2a*,
181 CD11c∆*Vhl*∆*Hif1a*∆*Hif2a* or their control Flox littermates in a 1:1 ratio (Figure 3C). After 1.5
182 months, similar numbers of total AMs were found in all the chimeric mice, ruling out differences
183 in niche accessibility (**Error! Reference source not found.**B). Frequencies of blood neutrophils
184 and monocytes from CD45.1$^+$CD45.2$^+$ and CD45.2$^+$ mice were also similar, indicating an equally
185 efficient bone marrow reconstitution (**Error! Reference source not found.**C,D). In the
186 bronchoalveolar lavage (BAL), CD45.2$^+$ CD11c∆*Vhl* and CD11c∆*Vhl*∆*Hif2a* monocyte-derived
187 AM were significantly less abundant than CD45.1$^+$CD45.2$^+$ control WT cells (Figure 3D),
188 correlating with a decreased frequency of Ki67$^+$ AMs (Figure 3E,F). Unexpectedly,
189 CD11c∆*Vhl*∆*Hif1a* monocyte-derived AM also showed a significantly reduced percentage of Ki67$^+$
190 cells but reconstituted the alveolar niche as efficiently as control WT AM, suggesting a survival
191 advantage (Figure 3D-F). These results indicate that while both HIF isoforms regulate AM self-

192 renewal capacity, HIF-1α overexpression may primarily underlie impaired alveolar niche
193 reconstitution upon pVHL absence.

194 In this bone marrow-graft model, CD11c∆*Vhl*, CD11c∆*Vhl*∆*Hif1a*, and CD11c∆*Vhl*∆*Hif2a*
195 monocyte-derived AMs expressed similar levels of CD11c (Figure 3G) but did not completely
196 restore CD45.1^{+}CD45.2^{+} WT control levels for Siglec-F, CD11b, and MHC class II (I-A/I-E) (Figure
197 3H-J). In contrast, AMs from WT littermates showed frequencies of Ki67^{+} and levels of surface
198 markers similar to CD45.1^{+}CD45.2^{+} WT controls (**Error! Reference source not found.**E-I). These
199 results confirm that the HIF-dependent defect in the maturation and proliferation of *Vhl*-deficient
200 AM is cell-intrinsic.

201 **HIF-2α selectively compromises surfactant clearance capacity by VHL-deficient AMs**
202 In lung alveoli, AMs play a major role degrading the surfactant produced by lung type II epithelial
203 cells. Genetic defects in GM-CSF signaling prevent AM maturation and lead to the development
204 of spontaneous PAP, characterized by the accumulation of surfactant.[30] HIF-1α mediated switch
205 to glycolysis has been linked to the accumulation of lipids and the development of foam cells. [31–
206 33] We previously reported that CD11c∆*Vhl* AMs have a decreased capacity to oxidize lipids *ex*
207 *vivo*, and consequently, when adoptively transferred to *Cfsr2*$^{-/-}$ mice, which lack AMs and develop
208 PAP spontaneously, they are not able to reduce the surfactant content in the alveoli.[10] To
209 interrogate on the regulation of lipid metabolism by HIF-1α or HIF-2α *in vivo*, we intratracheally
210 transferred AMs from CD11c∆*Vhl*∆*Hif1a*, CD11c∆*Vhl*∆*Hif2a*, CD11c∆*Vhl*∆*Hif1a*∆*Hif2a*, or their
211 control counterparts into *Cfsr2*$^{-/-}$ mice. Only adoptively transferred CD11c∆*Vhl*∆*Hif2a* AMs and
212 CD11c∆*Vhl*∆*Hif1a*∆*Hif2a* AMs were able to decrease total protein and specific SP-D protein in
213 BAL to levels similar to WT (Figure 4A,B), indicating that HIF-2α stabilization impairs surfactant
214 clearance by lung AMs. Similar numbers of AMs were recovered from BAL for all genotypes,
215 indicating the same efficiency at replenishing the lung alveoli (**Error! Reference source not**
216 **found.**A).

217 AMs rely on fatty-acid oxidation and cholesterol efflux to metabolize lipids and avoid their
218 accumulation respectively.[5] To assess the regulation of lipid oxidation by HIF isoforms in a
219 controlled *in vitro* setting, we conducted real-time metabolic profile with the fatty acid palmitoyl-
220 CoA as the only carbon source. BRR was significantly reduced in CD11c∆*Vhl* and
221 CD11c∆*Vhl*∆*Hif1a* AMs compared to WT but it was completely restored in CD11c∆*Vhl*∆*Hif2a* and
222 CD11c∆*Vhl*∆*Hif1a*∆*Hif2a* AMs (Figure 4C).

223 We then compared the expression of fatty acid and cholesterol metabolism related genes among
224 genotypes. In agreement with our *in vivo* and *in vitro* results, we found the expression of multiple
225 DEG associated with FA oxidation in *Vhl*-deficient AMs were commonly found in
226 CD11c∆*Vhl*∆*Hif1a* but WT expression profile was restored in CD11c∆*Vhl*∆*Hif2a* AM (Figure 4D).
227 Globally these results highlight HIF-2α is a major regulator of FA oxidation in lung AMs.

228 **DISCUSSION**

229 AMs are derived from embryonic progenitors that colonize the lung alveoli and mature after birth.
230 Maturation onset coincides with the exposure of the alveoli to high oxygen concentration upon
231 the first breath. We previously showed that genes related to the adaptation to hypoxia, including
232 HIF-target genes, are downregulated during AM maturation.[10] The role of HIF-1α is well studied
233 in monocyte-derived macrophages, where it plays a major role in macrophage infiltration and
234 proinflammatory responses.[34–38] Chronic and acute lung disease due to influenza infection
235 courses with lung edema and cellular infiltrations that can lead to hypoxia. [39,40] HIF-1α stabilization
236 has been reported in lung AMs upon lung injury associated to influenza infection, leading to
237 glycolysis induction.[41] However, the role of the HIF isoforms in AM metabolic adaptation to their
238 niche in homeostasis is largely unknown. In the present study, we have uncovered that HIF-1α
239 and HIF-2α differentially impair specific AM functions. Thus, the inactivation of HIF function is
240 essential for lung AM functional maturation. Our results demonstrate that HIF-1α is the exclusive
241 driver of the glycolytic switch in Vhl-deficient AMs. Notably, both HIF-1α and HIF-2α play a role in
242 the phenotypic maturation and transcriptional identity of AMs, corroborated by the cell-intrinsic
243 nature of the altered surface marker expression found in monocyte-derived AM deficient for Vhl,
244 Vhl/Hif1a and Vhl/Hif2a. HIF-1α stabilization leads to the expression of the antimicrobial enzyme
245 iNOS [42] and is protective against lung fibrosis.[26] This suggests that HIF activation in response to
246 certain exogenous stimuli can be beneficial, whereas under sterile conditions, HIF activity must
247 be tightly regulated.

248 Increased glycolysis has been linked with a decreased self-renewal potential in AMs.[5,43] Ki67
249 expression and BrdU uptake assays indicated that both HIF-1α and HIF-2α stabilization similarly
250 impair AM proliferation in the absence of pVHL. Despite the significant defect in proliferation of
251 *Vhl*-deficient AM, total numbers in the lung alveoli were similar to WT, suggesting that they can
252 fully replenish the alveolar niche in the absence of competition from incoming blood monocytes.
253 Indeed, our experiments with mixed bone marrow chimeras confirmed that that *Vhl*-deficient AM
254 defective proliferation is cell-intrinsic and that *Vhl*- and *Vhl*/*Hif2a*-deficient AMs are significantly
255 outcompeted by control WT AM. In contrast, *Vhl*/*Hif1a*-deficient AMs were similarly able to

repopulate the alveoli despite decreased Ki67 expression compared to control WT AM, what could be related with the pro-survival role of HIF-1α [41] although further investigation is required.

Notably, we found that compared to *Vhl/Hif1a*-deficient AMs, *Vhl/Hif2a*-deficient AMs had impaired oxidative capacity in the presence of glucose and glutamine as carbon source. In contrast, *Vhl/Hif1a*-deficient AMs showed a decreased oxygen consumption when using FA as carbon source, a phenomenon not observed in Vhl/Hif2a deficient AMs. Investigation on the specific roles of HIF-1α and HIF-2α in the regulation of lipid metabolism pathways is still controversial. HIF-2α has a dominant role leading to hepatic steatosis through fatty acid-oxidation impairment upon depletion of pVHL.[44] In contrast, HIF-1α was reported to enhance hepatic lipid accumulation in a model of alcoholic fatty liver disease.[32] Finally, another study shows that deletion both HIF isoforms is sufficient to ameliorate the lipid accumulation induced by hypoxia in HepG2 cell line.[45] The discrepancy among these results may rely on the different trigger used to activate HIF (pVHL depletion, alcohol and hypoxia, respectively), which likely involves a different dynamic of HIF isoform activation.[27] In the particular case of macrophages, the source of these cells may determine their metabolic requirements: monocyte derived macrophages (MDM) under hypoxia accumulate lipids and become foam cells, which correlates with the activation of HIF-1α.[31] HIF-1α can prevent cholesterol efflux contributing to lipid accumulation in a macrophage cell line.[33] However, MDM strongly rely on glycolysis compared to lung AM at a basal level,[46] suggesting that the metabolic regulation of MDMs cannot be extrapolated to tissue resident macrophages. In agreement, a recent study has shown that lung AMs are enriched in a fatty acid oxidation module including enzymes involved in lysosomal lipolysis, mitochondrial FA import and oxidation,[47] Our results unveil HIF-2α as the key regulator of lipid oxidation in lung AMs. *Vhl*/*Hif2a*-deficient AMs completely restore homeostatic levels of surfactant upon transfer to a mouse model of PAP and restore basal OCR levels when using Palmitoyl-CoA as substrate *in vitro*. In agreement, our transcriptional data shows multiple FA-related genes dysregulated in *Vhl*-deficient AMs, which were only restored upon further *Hif2a* inactivation. Overall, this work demonstrates the specific roles of HIF-1α and HIF-2α at fine-tuning lung AM gene expression and functions. Our results highlight the importance of developing therapies targeting each HIF isoform and unveil HIF-2α as a potential target to improve surfactant removal in secondary PAP diseases.

FIGURES

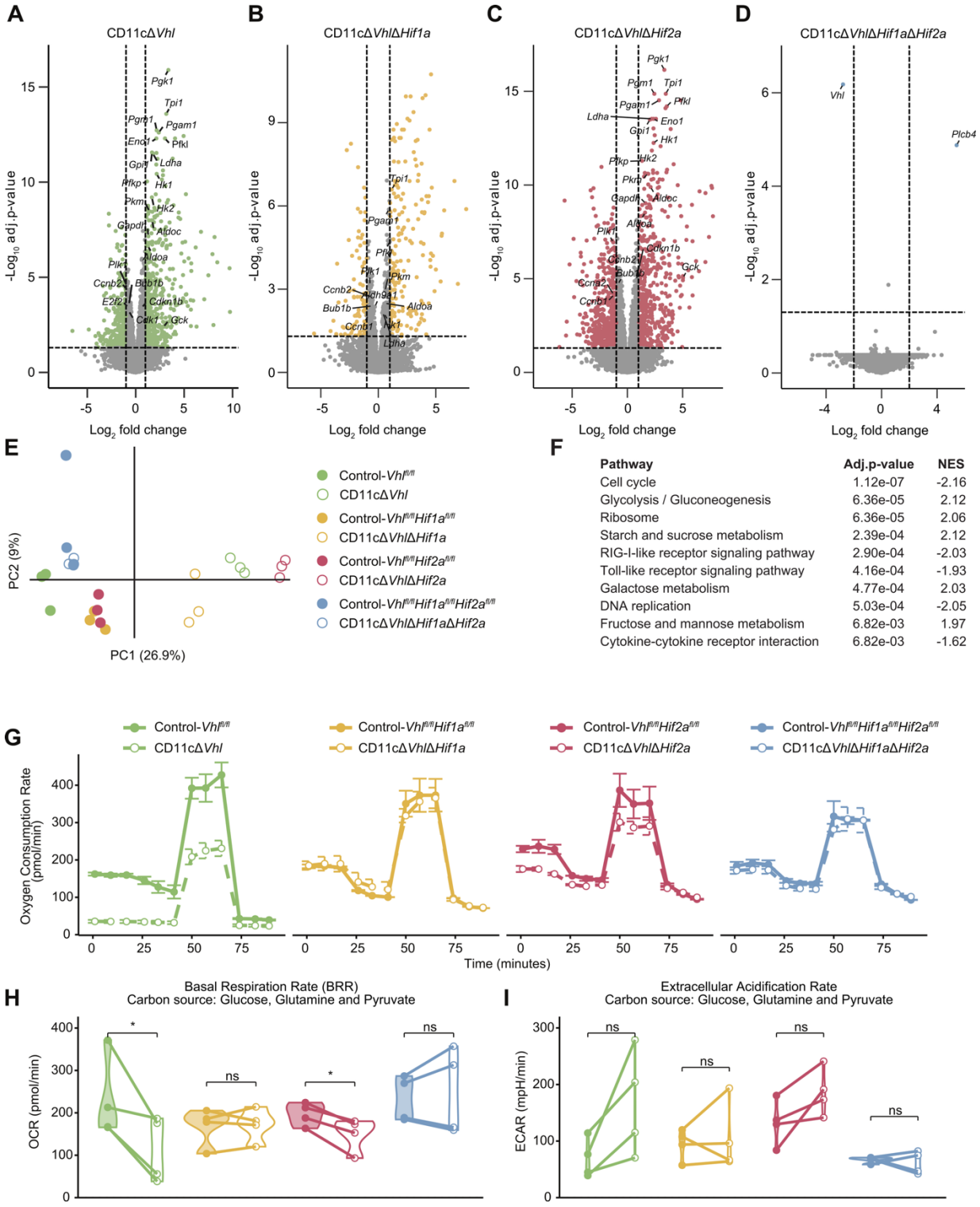

Pathway	Adj.p-value	NES
Cell cycle	1.12e-07	-2.16
Glycolysis / Gluconeogenesis	6.36e-05	2.12
Ribosome	6.36e-05	2.06
Starch and sucrose metabolism	2.39e-04	2.12
RIG-I-like receptor signaling pathway	2.90e-04	-2.03
Toll-like receptor signaling pathway	4.16e-04	-1.93
Galactose metabolism	4.77e-04	2.03
DNA replication	5.03e-04	-2.05
Fructose and mannose metabolism	6.82e-03	1.97
Cytokine-cytokine receptor interaction	6.82e-03	-1.62

Figure 1. HIF1α drives glycolysis in VHL-deficient alveolar macrophages.

(A-D) Volcano plot of differentially expressed genes ranked showing adjusted p-value (Log10 adj. p-value) and log2 fold change, between AMs from CD11c∆*Vhl* (A), CD11c∆*Vhl*∆*Hif1a* (B), CD11c∆*Vhl*∆*Hif2a* (C) and CD11c∆*Vhl*∆*Hif1a*∆*Hif2a* (D) mice compared to their littermate control; differentially expressed genes (adjusted p-value < 0.05 and abs(log2FC) > 1) are depicted in the color code associated with each genotype. (E) Principal component analysis (PCA) of transcriptomic profiles of AMs from CD11c∆*Vhl*, CD11c∆*Vhl*∆*Hif1a*, CD11c∆*Vhl*∆*Hif2a*, CD11c∆*Vhl*∆*Hif1a*∆*Hif2a* mice, and their littermate controls. Each dot represents a pull of 2-3 mice. (F) Pre-ranked enrichment analysis of the genes defining PC1 using KEGG Pathways. NES, normalized enrichment score; p-value adjusted with Benjamin–Hochberg correction. (G) Oxygen consumption rate (OCR) by BAL AMs cultured in media containing glucose, glutamine, and pyruvate. Data are shown as mean ± SD. (H, I) Basal respiratory rate (BRR) (H) and extracellular acidification rate (ECAR) (I) of BAL AMs. Each dot represents a pool of n = 6-7 mice per genotype. Paired Student's t-test, *p<0.05 and "ns" stands for non statistically significant. See also Figures S1, S2.

285

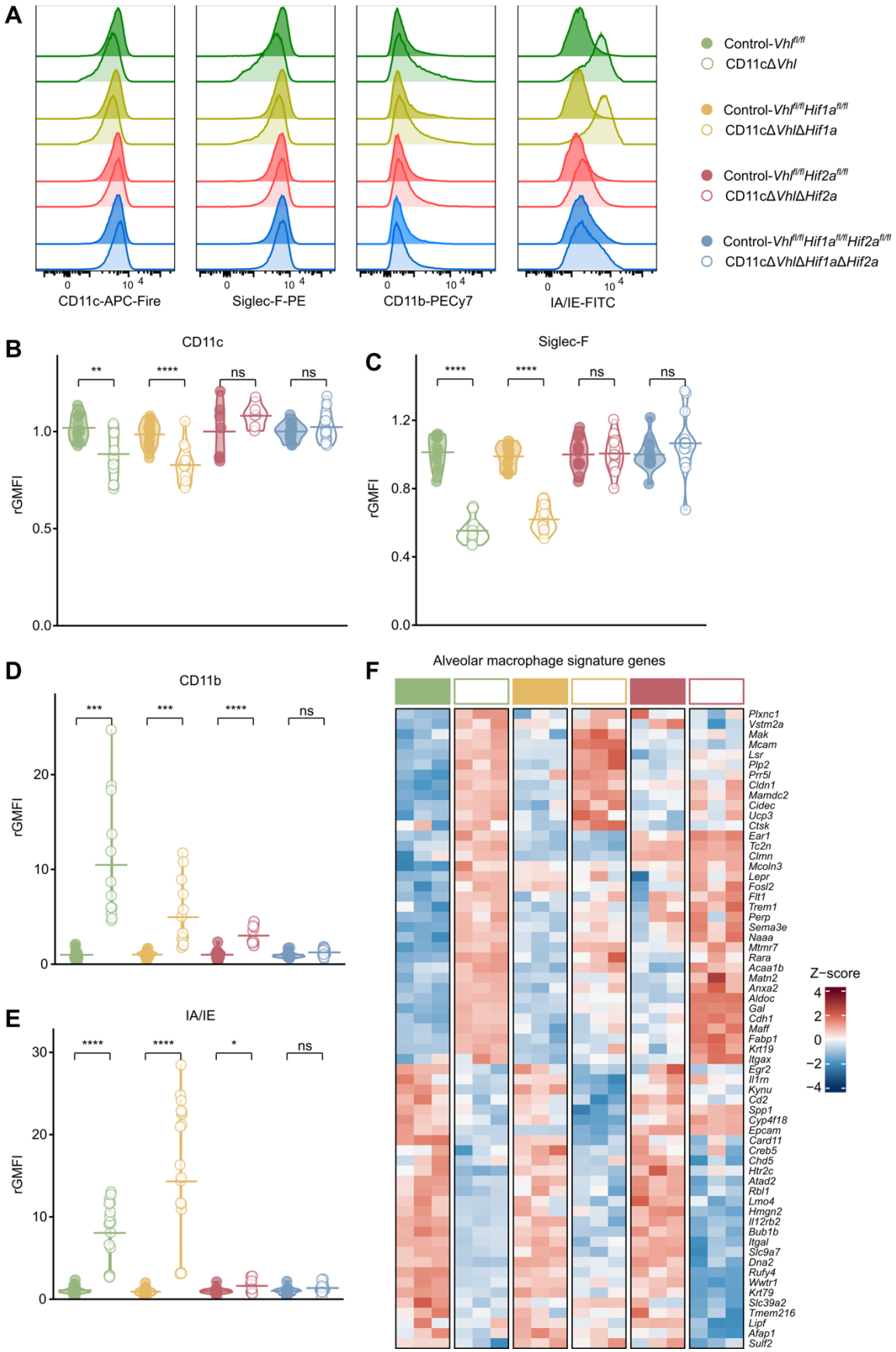
A
CD11c-APC-Fire
Siglec-F-PE
CD11b-PECy7
IA/IE-FITC
Control-Vhl fl/fl
CD11cΔVhl
Control-Vhl fl/fl Hif1a fl/fl
CD11cΔVhlΔHif1a
Control-Vhl fl/fl Hif2a fl/fl
CD11cΔVhlΔHif2a
Control-Vhl fl/fl Hif1a fl/fl Hif2a fl/fl
CD11cΔVhlΔHif1aΔHif2a
B
CD11c
rGMFI
C
Siglec-F
D
CD11b
E
IA/IE
F
Alveolar macrophage signature genes
Z−score
Plxnc1
Vstm2a
Mak
Mcam
Lsr
Plp2
Prr5l
Cldn1
Mamdc2
Cidec
Ucp3
Ctsk
Ear1
Tc2n
Clmn
Mcoln3
Lepr
Fosl2
Flt1
Trem1
Perp
Sema3e
Naaa
Mtmr7
Rara
Acaa1b
Matn2
Anxa2
Aldoc
Gal
Cdh1
Maff
Fabp1
Krt19
Itgax
Egr2
Il1rn
Kynu
Cd2
Spp1
Cyp4f18
Epcam
Card11
Creb5
Chd5
Htr2c
Atad2
Rbl1
Lmo4
Hmgn2
Il12rb2
Bub1b
Itgal
Slc9a7
Dna2
Rufy4
Wwtr1
Krt79
Slc39a2
Tmem216
Lipf
Afap1
Sulf2

Figure 2. Mature AM transcriptional signature relies on HIF inactivation.

(A) Representative flow cytometry histograms for CD11c, Siglec-F, CD11b and IA/IE expression by BAL AMs from the indicated genotypes. (B-E) Quantification of geometric mean of fluoresce intensity (GMFI) relative to the mean value of control samples (rGMFI) of CD11c (B), SiglecF (C), CD11b (D) and IA/IE (E). Pull of 2-3 experiments, n = 4-6 mice per experiment. Student's *t*-test, ****p<0.0001, ***p<0.001, **p<0.01 and "ns" stands for non-statistically significant. (F) Gene expression heatmap of the lung AM-specific signature gene set described in.[28]

286
287

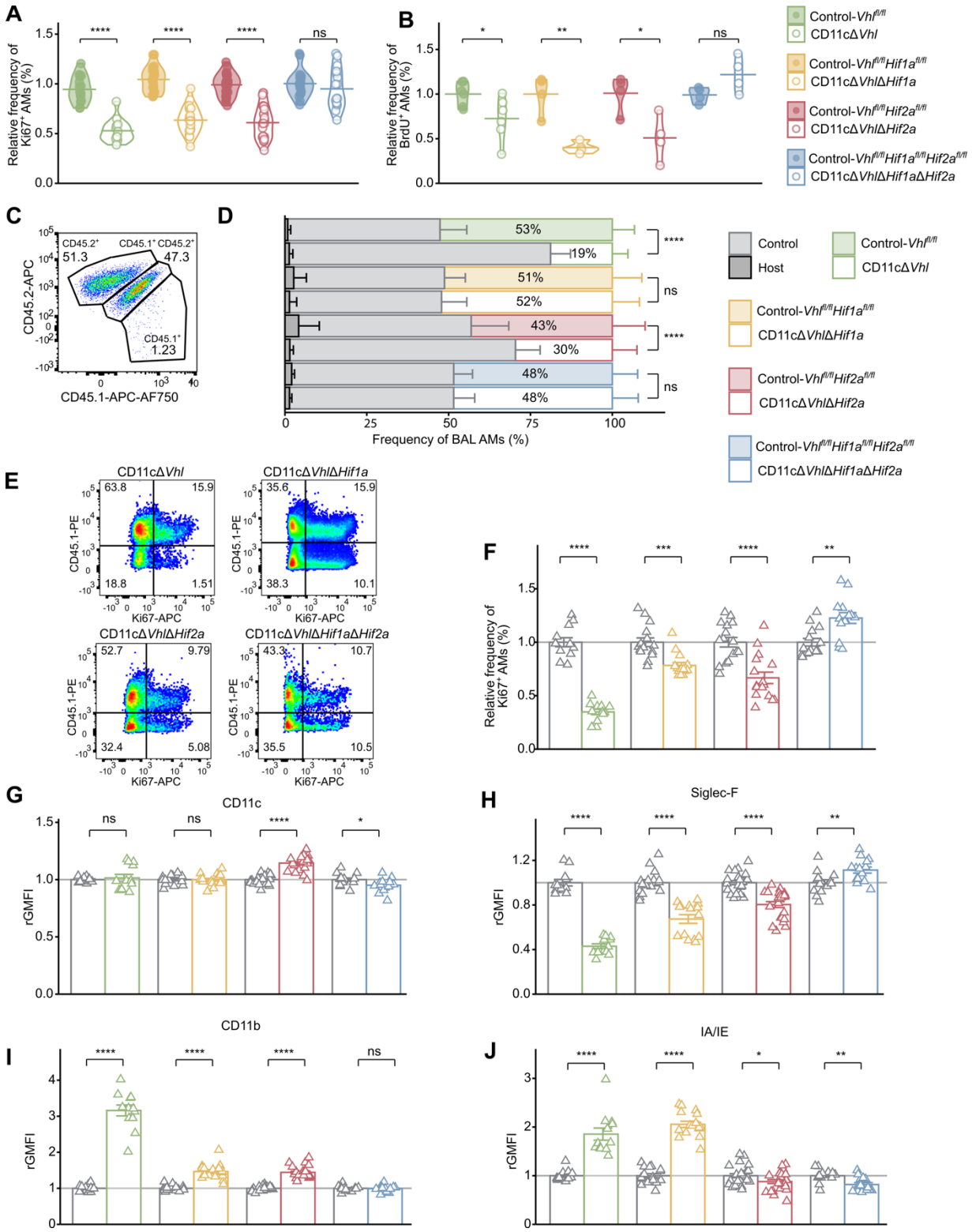

Figure 3. Both HIF isoforms interfere with AM self-renewal.

(A) Quantification of the frequency of Ki67+ BAL AMs relativized to the mean value for WT. Pull of 3 experiments, n= 5-8 mice per experiment. Student's *t*-test, ****p<0.0001, and "ns" stands

for non statistically significant. (B) Quantification of the frequency of BrdU+ BAL AMs after 3 days in culture with rGM-CSF. Pool of 2 experiments, each dot represents a pool of n = 15-18 mice per experiment . Student's *t*-test, **p<0.01, *p<0.05 and "ns" stands for non statistically significant. (C) Representative dot plot showing the percentage of host CD45.1$^+$, control transplanted CD45.1$^+$CD45.2$^+$ and experimental transplanted CD45.2$^+$ cells, gated within SiglecF$^+$ CD11c$^+$ BAL AMs (D) Quantification of the percentage of each AM subpopulation. Bar indicates mean ± SEM, Student's *t*-test, ****p<0.0001 and "ns" stands for non statistically significant. (E) Representative dot plots showing Ki67 expression by CD45.2$^+$ SiglecF$^+$CD11c$^+$ gated BAL AMs 45 days after BM transfer, in which CD45.1$^+$ and CD45.1$^-$ correspond to control and experimentally transplanted, respectively. (F) Quantification of the frequency of Ki67+ AMs of each genotype relativized to the mean value for control CD45.1$^+$ AMs. Bar indicates mean ± SEM, Student's *t*-test, ****p<0.0001, **p<0.01. (G-J) Quantification of geometric mean of fluoresce intensity (GMFI) relative to the mean value of control CD45.1$^+$ AMs samples (rGMFI) of CD11c (G), Siglec-F (H), CD11b (I) and IA/IE (J). Bar indicates mean ± SEM, Student's *t*-test, ****p<0.0001, **p<0.01, *p<0.05 and "ns" stands for non statistically significant. (D-J) Pool of experiments, n = 6-8 chimeras per experiment. See also Figure S3.

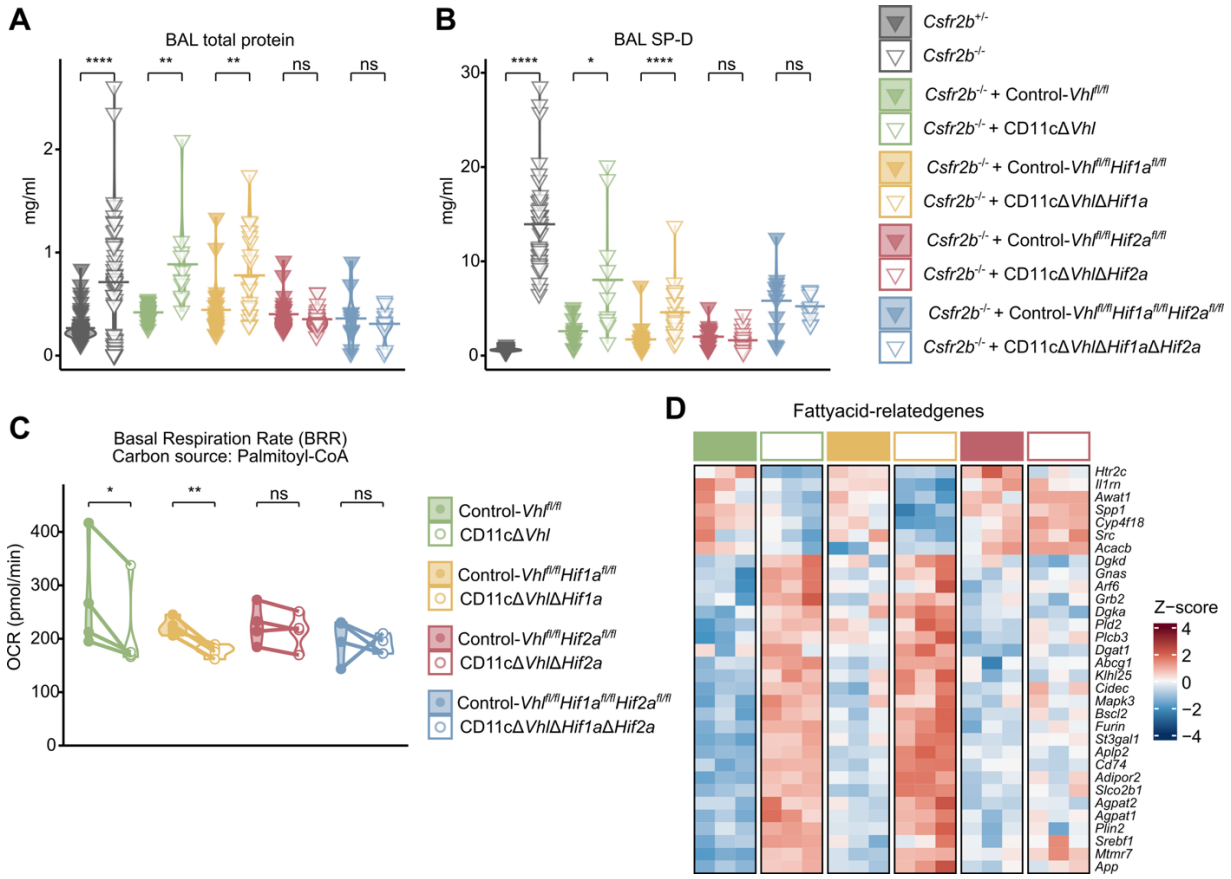

Figure 4. HIF-2 impairs fatty acid oxidation and surfactant clearance by AMs.

Quantification of total protein (A) and surfactant protein D (SP-D) (B) in BAL fluid from Csfr2b-/- mice transplanted with BAL AMs from the indicated genotypes. Control mice (Csfr2b$^{-/-}$ and Csfr2b$^{+/-}$) are pooled from each independent experiment. Pool of 3 experiments, n= 3-10 mice per experiment, Student's t-test, ****p<0.0001, **p<0.01, *p<0.05 and "ns" stands for non statistically significant. (C) Quantification of basal respiratory rate (BRR) of BAL AMs in media containing palmitoyl-CoA and L-carnitine. Pool of 4 experiments, each dot represents a pool of n=6-7 mice. Student's t-test, **p<0.01, *p<0.05 and "ns" stands for non statistically significant. (D) Heatmap showing differential expression of genes related to lipid metabolic process GO pathway (GO:0019216) in the indicated genotypes. See also figure S4.

288

289 **MATERIALS AND METHODS**

290 **Data.** RNA-seq data from Control-*Vhl* and CD11cΔVhl was previously published under GEO:
291 GSE108975 accession number. RNA-seq performed in this study has been deposited at GEO
292 and will be publicly available as of the date of publication (accession number).

293 **Mice.** Mice colonies were bred at Centro Nacional de Investigaciones Cardiovasculares Carlos
294 III (CNIC) under specific pathogen-free conditions. Experiments were conducted with 8- to 10-
295 weeks-old age-matched littermates (regardless of gender). Floxed *Vhl* mice were backcrossed
296 with or without floxed *Hif1a* and floxed *Hif2a*. Additionally, all possible combinations were
297 backcrossed with CD11c-Cre mice (B6.Cg-Tg(*Itgax*-cre)1-1Reiz/J) (kindly provided by Boris
298 Reizis) [48] in order to allow the targeting of the alveolar macrophage compartment. *Csf2rb*$^{-/-}$ mice
299 (kindly provided by Martin Guilliams),[49] and F1 from the mating between C57BL/6J mice
300 expressing the CD45.2 allele (Charles River) and B6/SJL (Ptprca Pepcb/BoyJ) mice expressing
301 the CD45.1 allele were also used. All experimental procedures were approved by the institutional
302 care and use committees and conformed to EU Directive 2010/63EU and Recommendation
303 2007/526/EC regarding the protection of animals used for experimental and other scientific
304 purposes, enforced in Spanish law under Royal Decree 53/2013.

305 **AM isolation.** Mice were sacrificed with a lethal dose of pentobarbital (Dolethal, Vetoquinol). To
306 isolate AMs for cell culture, ten bronchoalveolar lavages (BAL) were done by inserting a venal
307 catheter (18G BD Pharmingen) into the trachea with 1ml of phosphate-buffered saline (PBS), 5
308 mM EDTA, and 2 % inactivated fetal bovine serum (FBS, Sigma-Aldrich) (FACS buffer) at 37ºC.
309 Samples were kept on ice until further processing. BAL was centrifuged at 300xg for 10' at 4ºC
310 and red blood cell lysis was performed at room temperature (RT) for 3 min with RBC Lysis Buffer
311 (Sigma-Aldrich). Cells were resuspended in medium or FACs buffer depending on the application.

312 **AM *in vitro* culture.** AMs from BAL were cultured in RPMI 1640 (Gibco) supplemented with 10%
313 FBS, 100 U/ml Penicillin and Streptomycin (Lonza), 1mM Sodium Pyruvate (HyClone™), and 2
314 mM L-glutamine (complete RPMI) at 37ºC and 5% CO_2. For *in vitro* proliferation assay, cells were
315 supplemented with 10 pg/ml rGM-CSF (Peprotech). AMs were pulsed twice with BrdU (BD
316 Pharmingen) at 10μM: 10-12 h and 24h after culture onset. 24h after the second pulse, cells were
317 washed once with PBS to remove remaining FBS and incubated with accutase (StemCell
318 Technologies) for 15-20' at 37ºC. Cells were carefully detached by pipetting. After centrifugation
319 at 600 G for 5' at 4ºC, cells were resuspended and counted, and the same cell number per
320 condition and genotype was stained for surface markers and BrdU.

321 **Flow cytometry.** Single-cell suspensions were stained in 96-U-bottom plates. Surface staining
322 was performed in FACS buffer: PBS, 2.5 mM EDTA and 2.5% heat-inactivated FBS (iFBS).
323 Staining was performed for 15-20' at 4ºC with FcR block anti-mouse CD16/CD32 (2.4G2, Tonbo
324 Biosciences) and the appropriate mix of the following fluorochrome-conjugated antibodies in
325 FACS buffer: CD11c (clone HL3, BD Biosciences), Siglec-F (clone E50-2440, BD Biosciences),
326 CD64 (clone X54-5/7.1, BD Biosciences), CD11b (clone M1/70, BD Biosciences), F4/80 (clone
327 BM8, Life Technologies), MHCII (clone M5/114.15.2 BD Biosciences), Ly6G (clone 1A8, BD
328 Pharmingen), Ly6C (clone AL21, BD Biosciences), CD45 (30-F11, eBiosciences), CD45.1 (A20,
329 eBiosciences), CD45.2 (clone 104, BD Biosciences). Hoechst 33258 (Invitrogen) or Ghost Dye
330 Red 780 (Cell Signaling) were used as a counterstain to exclude dead cells. For intracellular Ki67
331 staining, AMs were stained for surface markers as described above, washed twice with FACs
332 buffer at 600 G for 5' at 4ºC, and mixed with unstained thymocytes, used as a cell carrier. Fixation
333 and permeabilization of cells were performed using the Foxp3/Transcription Factor Staining Buffer
334 Set (#00-5523-00, Invitrogen) and following manufacturer's instructions. Briefly, fixation solution
335 was prepared by diluting Fixation/Permeabilization concentrate, 1:3 with Fixation/Perm diluent.
336 Permeabilization buffer 10x was diluted 1:10 with sterile water and kept on ice. Cells were fixed
337 for 30' at 4ºC in the dark. Cells were washed with permeabilization buffer 1x and intracellular (i.c.)
338 staining was done right after. Intracellular staining with anti-Ki67-eFluor 660 (SolA15,
339 eBiosciences) or isotype control Rat IgG2aκ (eBR2a, eBiosciences) was performed in
340 permeabilization buffer 1x. All centrifugations after fixation were done at 1000 G for 5' at 4ºC.
341 Cells were resuspended in FACS buffer before acquisition. Intracellular BrdU staining was done
342 following manufacturer instructions. In brief, AMs were stained and mixed with carrier cells as
343 above-mentioned and fixed and permeabilized using the BrdU staining set (BD Pharmingen).
344 Cells were treated with DNAse and stained with anti-BrdU Ab (BD Pharmingen). Samples were
345 acquired in SP6800 Spectral, LSRFortessa, or FACSymphony cell analyzers, and data was
346 analyzed using FlowJo Version 10 software (Tree Star).

347 **Real-time oxygen consumption rate and glycolytic flux.** Real-time oxygen consumption rate
348 (OCR) and extracellular acidification rate (ECAR) were determined with Seahorse XF-96
349 Extracellular Flux Analyzer (Agilent Technologies). AMs from fresh BAL were pooled from 5-10
350 mice per genotype. After red blood cell lysis, $2.5x10^5$ AMs were plated in Cell-Tak (Corning)
351 coated wells. The assay was performed in DMEM supplemented with 100 µg/ml penicillin, 100
352 µg/ml streptomycin, and either 25 mM glucose, 1 mM pyruvate, and 2 mM glutamine or 5 mM L-
353 carnitine and 50 µM palmitoyl-CoA (all Sigma). pH was adjusted to 7.4 with KOH. Three
354 consecutive measurements were performed under basal conditions and after the sequential

355 addition of the following inhibitors: 1 μM Oligomycin, 1 μM Carbonyl cyanide 3-
356 chlorophenylhydrazone (CCCP), and 1 μM Rotenone with 1 μM Antimycin A. Basal respiratory
357 rate (BRR), maximal respiratory rate (MRR), spare respiratory capacity (SRC) and basal ECAR
358 were calculated according to Seahorse Agilent indications.

359 **RNA sequencing and analysis.** CD11c cell positive selection was performed on BAL
360 suspensions from 3-5 mice per genotype. Mouse CD11c MicroBeads UltraPure and MS columns
361 (all Miltenyi Biotec) were used according to manufacturers' instructions. Briefly, cells were
362 resuspended in 100 μL of FACS buffer plus 20 μL of CD11c MicroBeads, and incubated on ice
363 for 30 mins. Then, cells were washed and purified by magnetic positive selection with MS columns
364 (Miltenyi). A total of 3 pools of 3-5 mice per genotype were included. Total RNA was isolated using
365 Rneasy Micro Kit (Qiagen), and RNA quality was validated with a 2100 Bioanalyzer (Agilent).
366 RNA sequencing was performed in the Genomics Unit of the CNIC on Illumina HiSeq 2500
367 System. Sequencing reads were pre-processed through a pipeline that used FastQC to assess
368 read quality and Cutadapt to trim sequencing reads, eliminate Illumina adaptor remains, and
369 discard reads that were shorter than 30 base pairs. The resulting reads were mapped against the
370 mouse transcriptome (GRCm38.99) with STAR. Expected expressions were quantified using
371 RSEM, and batch normalization was applied with Combat as implemented in the sva R package.
372 Genes were filtered to have at least 10 CPM, and data were normalized using the trimmed mean
373 of m values (TMM), both with edgeR. DESeq2 rlog-normalized values were used to generate
374 Hexagonal Triwise diagrAMs with Triwise package. Significantly different genes for each pair-
375 wise comparison (p.adj < 0.05, logFC > 1.5) are displayed as red dots in the plots. Genes were
376 ranked according to log-Fold change, and gene set enrichment analysis was performed using
377 FGSEA algorithm and KEGG and GO databases. Redundant GO terms were removed using
378 GOSemSim package. Heatmaps display deregulated genes (Adj. p-value ≤ 0.05) of the specified
379 gene set.

380 For PCA-based enrichment analysis, $\log_2$(CPM) samples were scaled and used as input for
381 principal component analysis (PCA). Genes were ranked according to the loading vectors of PC1.
382 Resulting ranks were used as input for the FGSEA algorithm along with the Kyoto Encyclopedia
383 of Genes and Genomes (KEGG) (www.genome.jp/kegg) and Gene Ontology (GO)
384 (www.geneontology.org/) databases in order to identify the main sources of variability detected
385 by PCA. Only gene sets with a number of genes ≥ 15 and ≤ 500 were considered for PCA-based
386 enrichment analysis.

387 **Bone Marrow Transfer mixed chimeras.** B6/SJL mice expressing the CD45.1 congenic marker
388 were lethally irradiated with 2 doses of 6 Gy that were 3 hours apart and reconstituted
389 intravenously with $5x10^6$ cells of a 1:1 mixture of $CD45.1^+$ $CD45.2^+$ wild-type BM cells and
390 $CD45.2^+$ BM cells coming from the indicated experimental genotypes. Mice were analyzed 45-50
391 days after reconstitution as previously described. A small sample of peripheral blood was
392 harvested one day before the experimental endpoint to test immune compartment reconstitution.

393 **Pulmonary macrophage transplantation.** $5x10^4$ AMs from BAL were transferred intratracheally
394 into $Csf2rb^{-/-}$ mice. Recipient mice were anesthetized with Ketamine (Imalgene, Merial) and
395 Xylazine (Rompun, Bayer). When entirely unconscious, a small incision was made to partially
396 expose the trachea. Then, mice were carefully intubated orotracheally with an IV catheter (22 G;
397 BD Insyte). Cells were inoculated with a pipette in 30µl of PBS. Next, mice were extubated, and
398 the incision sutured. Mice were finally injected with anesthesia reversor (Medeson, Urano) and
399 kept in a warm plaque until complete recovery. 1ml PBS1x-BAL from recipient mice was collected
400 six weeks after transplantation. Cells were centrifuged at 1700 rpm for 5 min at RT and
401 supernatant was used to measure total protein concentration by BCA (Pierce BCA Protein Assay
402 Kit, Thermo Scientific) and surfactant protein D (SP-D) concentration by ELISA (SP-D DUO ELISA
403 kit, R&D System), according to the manufacturer's instruction. Cell engraftment was compared
404 by flow cytometry of total lung cells.

405 **Statistical analysis.** Statistical comparisons were analyzed using R v.4.2.1. Data are presented
406 as individual values and were analyzed as indicated in the legends or the dedicated methods
407 section. All experiments were repeated at least twice, and pooled data from several experiments
408 are shown as indicated in the legends. All *n* values represent biological replicates (different mice,
409 primary cell preparations, or in vitro experiments). Differences were considered significant when
410 $p \leq 0.05$ and are indicated as *ns* when not significant, $*p \leq 0.05$, $**p \leq 0.01$, $***p \leq 0.001$, $****p \leq$
411 0.0001.

412

413 **ACKNOWLEDGEMENTS**

414 We thank members of the DS laboratory at CNIC, past and present, for feedback and scientific
415 discussions on this project and manuscript. Thanks also to all CNIC facilities and assistants for
416 their support. Work in the DS laboratory is funded by the CNIC; by Ministerio de Ciencia,
417 Innovación y Universidades (MICIU) PID2022-137712OB-I00, CPP2021-008310 and CPP2022-
418 009762 MICIU/AEI/10.13039/501100011033 Agencia Estatal de Investigación, Unión Europea

419 NextGenerationEU/PRTR; by Comunidad de Madrid (P2022/BMD-7333 INMUNOVAR-CM); by
420 Scientific Foundation of the Spanish Association Against Cancer (AECC- PRYGN246642SANC);
421 by Worldwide Cancer Research WWCR-25-0080; by European Union ERC-2023-PoC; by a
422 research agreement with Inmunotek S.L.; and by “la Caixa” Foundation (LCF/PR/HR23/52430012
423 and LCF/PR/HR22/52420019).

424 The CNIC is supported by the Instituto de Salud Carlos III (ISCIII), the MICIU and the Pro CNIC
425 Foundation, and is a Severo Ochoa Center of Excellence (CEX2020-001041-S funded by
426 MICIU/AEI /10.13039/501100011033).

REFERENCES

1. Hashimoto, D., Chow, A., Noizat, C., Teo, P., Beasley, M.B., Leboeuf, M., Becker, C.D., See, P., Price, J., Lucas, D., et al. (2013). Tissue-Resident Macrophages Self-Maintain Locally throughout Adult Life with Minimal Contribution from Circulating Monocytes. Immunity *38*, 792–804. https://doi.org/10.1016/j.immuni.2013.04.004.

2. Guilliams, M., De Kleer, I., Henri, S., Post, S., Vanhoutte, L., De Prijck, S., Deswarte, K., Malissen, B., Hammad, H., and Lambrecht, B.N. (2013). Alveolar macrophages develop from fetal monocytes that differentiate into long-lived cells in the first week of life via GM-CSF. J. Exp. Med. *210*, 1977–1992. https://doi.org/10.1084/jem.20131199.

3. Schneider, C., Nobs, S.P., Kurrer, M., Rehrauer, H., Thiele, C., and Kopf, M. (2014). Induction of the nuclear receptor PPAR-γ by the cytokine GM-CSF is critical for the differentiation of fetal monocytes into alveolar macrophages. Nat. Immunol. *15*, 1026–1037. https://doi.org/10/f6msqc.

4. Evren, E., Ringqvist, E., and Willinger, T. (2020). Origin and ontogeny of lung macrophages: from mice to humans. Immunology *160*, 126–138. https://doi.org/10.1111/imm.13154.

5. Wculek, S.K., Heras-Murillo, I., Mastrangelo, A., Mañanes, D., Galán, M., Miguel, V., Curtabbi, A., Barbas, C., Chandel, N.S., Enríquez, J.A., et al. (2023). Oxidative phosphorylation selectively orchestrates tissue macrophage homeostasis. Immunity *56*, 516-530.e9. https://doi.org/10.1016/j.immuni.2023.01.011.

6. Fujii, W., Kapellos, T.S., Baßler, K., Händler, K., Holsten, L., Knoll, R., Warnat-Herresthal, S., Oestreich, M., Hinkley, E.R., Hasenauer, J., et al. (2021). Alveolar macrophage transcriptomic profiling in COPD shows major lipid metabolism changes. ERJ Open Res. *7*. https://doi.org/10.1183/23120541.00915-2020.

7. Robb, L. (1995). Hematopoietic and lung abnormalities in mice with a null mutation of the common f3 subunit of the receptors for granulocyte-macrophage colony-stimulating factor and interleukins 3 and 5. Proc Natl Acad Sci USA, 5. https://doi.org/10/b7ckwn.

8. Stanley, E., Lieschke, G.J., Grail, D., Metcalf, D., Hodgson, G., Gall, J.A., Maher, D.W., Cebon, J., Sinickas, V., and Dunn, A.R. (1994). Granulocyte/macrophage colony-stimulating factor-deficient mice show no major perturbation of hematopoiesis but develop a characteristic pulmonary pathology. Proc. Natl. Acad. Sci. *91*, 5592–5596. https://doi.org/10/cz3dc3.

9. Gao, X., Zhu, B., Wu, Y., Li, C., Zhou, X., Tang, J., and Sun, J. (2022). TFAM-Dependent Mitochondrial Metabolism Is Required for Alveolar Macrophage Maintenance and Homeostasis. J. Immunol. *208*, 1456–1466. https://doi.org/10.4049/jimmunol.2100741.

10. Izquierdo, H.M., Brandi, P., Gómez, M.-J., Conde-Garrosa, R., Priego, E., Enamorado, M., Martínez-Cano, S., Sánchez, I., Conejero, L., Jimenez-Carretero, D., et al. (2018). Von Hippel-Lindau Protein Is Required for Optimal Alveolar Macrophage Terminal Differentiation, Self-Renewal, and Function. Cell Rep. *24*, 1738–1746. https://doi.org/10.1016/j.celrep.2018.07.034.

11. Iliopoulos, O., Levy, A.P., Jiang, C., Kaelin, W.G., and Goldberg, M.A. (1996). Negative regulation of hypoxia-inducible genes by the von Hippel-Lindau protein. Proc. Natl. Acad. Sci. *93*, 10595–10599. https://doi.org/10.1073/pnas.93.20.10595.

12. Maxwell, P.H., Wiesener, M.S., Chang, G.-W., Clifford, S.C., Vaux, E.C., Cockman, M.E., Wykoff, C.C., Pugh, C.W., Maher, E.R., and Ratcliffe, P.J. (1999). The tumour suppressor protein VHL targets hypoxia-inducible factors for oxygen-dependent proteolysis. Nature *399*, 271–275. https://doi.org/10.1038/20459.

13. Stebbins, C.E., Kaelin, W.G., and Pavletich, N.P. (1999). Structure of the VHL-ElonginC-ElonginB complex: implications for VHL tumor suppressor function. Science *284*, 455–461. https://doi.org/10.1126/science.284.5413.455.

14. Kaelin, W.G. (2022). Von Hippel–Lindau disease: insights into oxygen sensing, protein degradation, and cancer. J. Clin. Invest. *132*. https://doi.org/10.1172/JCI162480.

15. Wang, G.L., Jiang, B.H., Rue, E.A., and Semenza, G.L. (1995). Hypoxia-inducible factor 1 is a basic-helix-loop-helix-PAS heterodimer regulated by cellular O2 tension. Proc. Natl. Acad. Sci. *92*, 5510–5514. https://doi.org/10.1073/pnas.92.12.5510.

16. Koh, M.Y., and Powis, G. (2012). Passing the baton: the HIF switch. Trends Biochem. Sci. *37*, 364–372. https://doi.org/10.1016/j.tibs.2012.06.004.

17. Yang, S.-L., Wu, C., Xiong, Z.-F., and Fang, X. (2015). Progress on hypoxia-inducible factor-3: Its structure, gene regulation and biological function (Review). Mol. Med. Rep. *12*, 2411–2416. https://doi.org/10.3892/mmr.2015.3689.

18. Hu, L., Xie, H., Liu, X., Potjewyd, F., James, L.I., Wilkerson, E.M., Herring, L.E., Xie, L., Chen, X., Cabrera, J.C., et al. (2020). TBK1 Is a Synthetic Lethal Target in Cancer with *VHL* Loss. Cancer Discov. *10*, 460–475. https://doi.org/10.1158/2159-8290.CD-19-0837.

19. Frew, I.J., and Krek, W. (2008). pVHL: A Multipurpose Adaptor Protein. Sci. Signal. *1*. https://doi.org/10/dg4k3s.

20. Ji, Q., and Burk, R.D. (2008). Downregulation of integrins by von Hippel-Lindau (VHL) tumor suppressor protein is independent of VHL-directed hypoxia-inducible factor alpha degradation. Biochem. Cell Biol. *86*, 227–234. https://doi.org/10.1139/O08-035.

21. Yang, H., Minamishima, Y.A., Yan, Q., Schlisio, S., Ebert, B.L., Zhang, X., Zhang, L., Kim, W.Y., Olumi, A.F., and Kaelin, W.G. (2007). pVHL Acts as an Adaptor to Promote the Inhibitory Phosphorylation of the NF-κB Agonist Card9 by CK2. Mol. Cell *28*, 15–27. https://doi.org/10.1016/j.molcel.2007.09.010.

22. Hergovich, A., Lisztwan, J., Barry, R., Ballschmieter, P., and Krek, W. (2003). Regulation of microtubule stability by the von Hippel-Lindau tumour suppressor protein pVHL. Nat. Cell Biol. *5*, 64–70. https://doi.org/10.1038/ncb899.

23. Li, S., Li, W., Yuan, J., Bullova, P., Wu, J., Zhang, X., Liu, Y., Plescher, M., Rodriguez, J., Bedoya-Reina, O.C., et al. (2022). Impaired oxygen-sensitive regulation of mitochondrial biogenesis within the von Hippel–Lindau syndrome. Nat. Metab. *4*, 739–758. https://doi.org/10.1038/s42255-022-00593-x.

24. Briston, T., Stephen, J.M., Thomas, L.W., Esposito, C., Chung, Y.-L., Syafruddin, S.E., Turmaine, M., Maddalena, L.A., Greef, B., Szabadkai, G., et al. (2018). VHL-Mediated Regulation of CHCHD4 and Mitochondrial Function. Front. Oncol. *8*, 1–16. https://doi.org/10.3389/fonc.2018.00388.

25. Zhu, S., Ding, W., Chen, Y., Wang, W., Xu, R., Liu, C., Liu, X., and Deng, H. (2022). High *VHL* Expression Reverses Warburg Phenotype and Enhances Immunogenicity in Kidney Tumor Cells. Genomics Proteomics Bioinformatics *20*, 657–669. https://doi.org/10.1016/j.gpb.2019.12.002.

26. Zhang, W., Li, Q., Li, D., Li, J., Aki, D., and Liu, Y.-C. (2018). The E3 ligase VHL controls alveolar macrophage function via metabolic–epigenetic regulation. J. Exp. Med. *215*, 3180–3193. https://doi.org/10.1084/jem.20181211.

27. Jaśkiewicz, M., Moszyńska, A., Króliczewski, J., Cabaj, A., Bartoszewska, S., Charzyńska, A., Gebert, M., Dąbrowski, M., Collawn, J.F., and Bartoszewski, R. (2022). The transition from HIF-1 to HIF-2

511 during prolonged hypoxia results from reactivation of PHDs and HIF1A mRNA instability. Cell. Mol.
512 Biol. Lett. *27*, 109. https://doi.org/10.1186/s11658-022-00408-7.

513 28. Gautier, E.L., Shay, T., Miller, J., Greter, M., Jakubzick, C., Ivanov, S., Helft, J., Chow, A., Elpek, K.G.,
514 Gordonov, S., et al. (2012). Gene-expression profiles and transcriptional regulatory pathways that
515 underlie the identity and diversity of mouse tissue macrophages. Nat. Immunol. *13*, 1118–1128.
516 https://doi.org/10.1038/ni.2419.

517 29. van de Laar, L., Saelens, W., De Prijck, S., Martens, L., Scott, C.L., Van Isterdael, G., Hoffmann, E.,
518 Beyaert, R., Saeys, Y., Lambrecht, B.N., et al. (2016). Yolk Sac Macrophages, Fetal Liver, and Adult
519 Monocytes Can Colonize an Empty Niche and Develop into Functional Tissue-Resident Macrophages.
520 Immunity *44*, 755–768. https://doi.org/10/f8kzs9.

521 30. Huang, X., Cao, M., and Xiao, Y. (2023). Alveolar macrophages in pulmonary alveolar proteinosis:
522 origin, function, and therapeutic strategies. Front. Immunol. *14*, 1195988.
523 https://doi.org/10.3389/fimmu.2023.1195988.

524 31. Crucet, M., Wüst, S.J.A., Spielmann, P., Lüscher, T.F., Wenger, R.H., and Matter, C.M. (2013). Hypoxia
525 enhances lipid uptake in macrophages: role of the scavenger receptors Lox1, SRA, and CD36.
526 Atherosclerosis *229*, 110–117. https://doi.org/10.1016/j.atherosclerosis.2013.04.034.

527 32. Nath, B., Levin, I., Csak, T., Petrasek, J., Mueller, C., Kodys, K., Catalano, D., Mandrekar, P., and
528 Szabo, G. (2011). Hepatocyte-specific hypoxia-inducible factor-1α is a determinant of lipid
529 accumulation and liver injury in alcohol-induced steatosis in mice. Hepatol. Baltim. Md *53*, 1526–1537.
530 https://doi.org/10.1002/hep.24256.

531 33. Parathath, S., Mick, S.L., Feig, J.E., Joaquin, V., Grauer, L., Habiel, D.M., Gassmann, M., Gardner,
532 L.B., and Fisher, E.A. (2011). Hypoxia is present in murine atherosclerotic plaques and has multiple
533 adverse effects on macrophage lipid metabolism. Circ. Res. *109*, 1141–1152.
534 https://doi.org/10.1161/CIRCRESAHA.111.246363.

535 34. Cramer, T., Yamanishi, Y., Clausen, B.E., Forster, I., Pawlinski, R., Mackman, N., Haase, V.H.,
536 Jaenisch, R., Corr, M., Nizet, V., et al. (2003). HIF-1 alpha is essential for myeloid cell-mediated
537 inflammation (vol 112, pg 648, 2003). Cell *113*, 419.

538 35. Matak, P., Heinis, M., Mathieu, J.R.R., Corriden, R., Cuvellier, S., Delga, S., Mounier, R., Rouquette,
539 A., Raymond, J., Lamarque, D., et al. (2015). Myeloid HIF-1 is protective in Helicobacter pylori-
540 mediated gastritis. J. Immunol. Baltim. Md 1950 *194*, 3259–3266.
541 https://doi.org/10.4049/jimmunol.1401260.

542 36. Palsson-McDermott, E.M., Curtis, A.M., Goel, G., Lauterbach, M.A.R., Sheedy, F.J., Gleeson, L.E.,
543 van den Bosch, M.W.M., Quinn, S.R., Domingo-Fernandez, R., Johnson, D.G.W., et al. (2015).
544 Pyruvate Kinase M2 Regulates Hif-1α Activity and IL-1β Induction and Is a Critical Determinant of the
545 Warburg Effect in LPS-Activated Macrophages. Cell Metab. *21*, 65–80.
546 https://doi.org/10.1016/j.cmet.2014.12.005.

547 37. Peyssonnaux, C., Datta, V., Cramer, T., Doedens, A., Theodorakis, E.A., Gallo, R.L., Hurtado-Ziola,
548 N., Nizet, V., and Johnson, R.S. (2005). HIF-1α expression regulates the bactericidal capacity of
549 phagocytes. J. Clin. Invest. *115*, 1806–1815. https://doi.org/10.1172/JCI23865.

550 38. Tannahill, G.M., Curtis, A.M., Adamik, J., Palsson-McDermott, E.M., McGettrick, A.F., Goel, G., Frezza,
551 C., Bernard, N.J., Kelly, B., Foley, N.H., et al. (2013). Succinate is an inflammatory signal that induces
552 IL-1β through HIF-1α. Nature *496*, 238–242. https://doi.org/10.1038/nature11986.

553 39. Schaible, B., Schaffer, K., and Taylor, C.T. (2010). Hypoxia, innate immunity and infection in the lung.
554 Respir. Physiol. Neurobiol. *174*, 235–243. https://doi.org/10.1016/j.resp.2010.08.006.

555 40. Traylor, Z.P., Aeffner, F., and Davis, I.C. (2013). Influenza A H1N1 induces declines in alveolar gas
556 exchange in mice consistent with rapid post-infection progression from acute lung injury to ARDS.
557 Influenza Other Respir. Viruses *7*, 472–479. https://doi.org/10.1111/j.1750-2659.2012.00414.x.

558 41. Woods, P.S., Kimmig, L.M., Sun, K.A., Meliton, A.Y., Shamaa, O.R., Tian, Y., Cetin-Atalay, R.,
559 Sharp, W.W., Hamanaka, R.B., and Mutlu, G.M. (2022). HIF-1α induces glycolytic reprograming in
560 tissue-resident alveolar macrophages to promote cell survival during acute lung injury. eLife *11*,
561 e77457. https://doi.org/10.7554/eLife.77457.

562 42. Aki, D., Li, Q., Li, H., Liu, Y.-C., and Lee, J.H. (2019). Immune regulation by protein ubiquitination:
563 roles of the E3 ligases VHL and Itch. Protein Cell *10*, 395–404. https://doi.org/10.1007/s13238-018-
564 0586-8.

565 43. Zhu, B., Wu, Y., Huang, S., Zhang, R., Son, Y.M., Li, C., Cheon, I.S., Gao, X., Wang, M., Chen, Y., et
566 al. (2021). Uncoupling of macrophage inflammation from self-renewal modulates host recovery from
567 respiratory viral infection. Immunity *54*, 1200-1218.e9. https://doi.org/10/gjvz72.

568 44. Rankin, E.B., Rha, J., Selak, M.A., Unger, T.L., Keith, B., Liu, Q., and Haase, V.H. (2009). Hypoxia-
569 inducible factor 2 regulates hepatic lipid metabolism. Mol. Cell. Biol. *29*, 4527–4538.
570 https://doi.org/10.1128/MCB.00200-09.

571 45. Liu, Y., Ma, Z., Zhao, C., Wang, Y., Wu, G., Xiao, J., McClain, C.J., Li, X., and Feng, W. (2014). HIF-
572 1α and HIF-2α are critically involved in hypoxia-induced lipid accumulation in hepatocytes through
573 reducing PGC-1α-mediated fatty acid β-oxidation. Toxicol. Lett. *226*, 117–123.
574 https://doi.org/10.1016/j.toxlet.2014.01.033.

575 46. Wood, E.G., Macdougall, C.E., Blythe, H., Clément, M., Colas, R.A., Dalli, J., Marelli-Berg, F., and
576 Longhi, M.P. (2020). HIF1α activation in dendritic cells under sterile conditions promotes an anti-
577 inflammatory phenotype through accumulation of intracellular lipids. Sci. Rep. *10*, 1–12.
578 https://doi.org/10.1038/s41598-020-77793-6.

579 47. Gainullina, A., Mogilenko, D.A., Huang, L.-H., Todorov, H., Narang, V., Kim, K.-W., Yng, L.S., Kent,
580 A., Jia, B., Seddu, K., et al. (2023). Network analysis of large-scale ImmGen and Tabula Muris
581 datasets highlights metabolic diversity of tissue mononuclear phagocytes. Cell Rep. *42*, 112046.
582 https://doi.org/10.1016/j.celrep.2023.112046.

583 48. Caton, M.L., Smith-Raska, M.R., and Reizis, B. (2007). Notch–RBP-J signaling controls the
584 homeostasis of CD8− dendritic cells in the spleen. J. Exp. Med. *204*, 1653–1664.
585 https://doi.org/10.1084/jem.20062648.

586 49. Robb, L., Drinkwater, C.C., Metcalf, D., Li, R., Köntgen, F., Nicola, N.A., and Begley, C.G. (1995).
587 Hematopoietic and lung abnormalities in mice with a null mutation of the common beta subunit of the
588 receptors for granulocyte-macrophage colony-stimulating factor and interleukins 3 and 5. Proc. Natl.
589 Acad. Sci. *92*, 9565–9569. https://doi.org/10.1073/pnas.92.21.9565.

590